Price, A.T., 1949. The induction of electric currents in nonuniform thin sheets and shells. *Quarterly Journal of Mechanics and Applied Mathematics*, **2**: 283–310.
Price, A.T., 1950. Electromagnetic induction in a semi-infinite conductor with a plane boundary. *Quarterly Journal of Mechanics and Applied Mathematics*, **3**: 385–410.
Price, A.T., 1962. Theory of magnetotelluric methods when the source field is considered. *Journal of Geophysical Research*, **67**: 1907–1918.
Price, A.T., 1967a. Electromagnetic Induction within the Earth. In Matsushita, S., and Campbell, W.H. (eds.), *Physics of Geomagnetic Phenomena.* London and New York: Academic Press, pp. 235–295.
Price, A.T., 1967b. Magnetic Variations and Telluric Currents. In Gaskell, T.F. (ed.), *The Earth's Mantle.* London and New York: Academic Press, pp. 125–170.
Price, A.T., and Chapman, S., 1928. On line-integrals of the diurnal magnetic variations. *Proceedings of the Royal Society of London*, A**119**: 182–196.
Price, A.T., and Stone, D.J., 1964. The quiet day magnetic variations during the IGY. In *Annals of the International Geophysical Year*, **35** Part III.
Price, A.T., and Wilkins, G.A., 1963. New methods for the analysis of geomagnetic fields and their application to the Sq field of 1932–1933. *Philosophical Transactions of the Royal Society of London*, A**256**: 31–98.

Cross-references:

Chapman, Sydney (1888–1970)
Ionosphere
Magnetotellurics
Mantle, Electrical Conductivity, Mineralogy
Ocean, Electromagnetic Effects
Storms and Substorms, Magnetic

PRINCIPAL COMPONENT ANALYSIS IN PALEOMAGNETISM

When studying the mean and variance of paleomagnetic data it is a common practice to employ principal component analysis (Jolliffe, 2002). The theory of this method is related to the mathematics quantifying the moment of inertia of a set of particles of mass about some reference point of interest. For the purposes of data analysis, principal component analysis was first promoted by Pearson (1901) and Hotelling (1933), and it also often associated with Karhunen (1947) and Loéve (1977). Principal component analysis is widely applied in crystallography (e.g., Schomaker *et al*., 1959). In paleomagnetism (e.g., Mardia, 1972; Kirschvink, 1980), it finds application in studies of the average paleofield, paleosecular variation, demagnetization, and magnetic susceptibility. Here we discuss and demonstrate principal component analysis in application to full paleomagnetic vectorial data and, separately, to paleomagnetic directional data.

Vectorial analysis

Consider a set of paleomagnetic vectors, with the ith vector $\mathbf{x}(i)$ having intensity, inclination, and declination values ($F(i)$, $I(i)$, $D(i)$). Their equivalent Cartesian expression is just

$$\begin{aligned} x_1(i) &= F(i)\cos I(i)\cos D(i),\\ x_2(i) &= F(i)\cos I(i)\sin D(i),\\ x_3(i) &= F(i)\sin I(i), \end{aligned} \qquad \text{(Eq. 1)}$$

where $\mathbf{x} = (x_1, x_2, x_3)$ represents the usual geographic components of (north, east, down). With N such vectorial data we can calculate their values relative to some fixed reference point $\mathbf{r} = (r_1, r_2, r_3)$

$$\delta\mathbf{x}(i) = \mathbf{x}(i) - \mathbf{r} \qquad \text{(Eq. 2)}$$

and with which we can calculate their covariance matrix,

$$\mathrm{C} = \frac{1}{N}\begin{pmatrix} \sum \delta x_1(i)^2 & \sum \delta x_1(i)\delta x_2(i) & \sum \delta x_1(i)\delta x_3(i) \\ \sum \delta x_2(i)\delta x_1(i) & \sum \delta x_2(i)^2 & \sum \delta x_2(i)\delta x_3(i) \\ \sum \delta x_3(i)\delta x_1(i) & \sum \delta x_3(i)\delta x_2(i) & \sum \delta x_3(i)^2 \end{pmatrix}. \qquad \text{(Eq. 3)}$$

This matrix can be reduced to diagonal form by an appropriate choice of axes, obtained by solving the eigenvalue problem

$$\mathrm{C}\mathbf{e}^m = \lambda_m \mathbf{e}^m, \qquad \text{(Eq. 4)}$$

where $\mathbf{e}^m$ is an eigenvector and λ_m is an eigenvalue (e.g., Strang, 1980). Three eigenvectors $\mathbf{e}^m$, for $m = 1, 2, 3$, and their corresponding eigenvalues λ_m can be found using standard numerical packages, such as LAPACK. The eigenvectors are orthogonal, and therefore

$$\mathbf{e}^m \cdot \mathbf{e}^n = 0, \quad \text{for} \quad m \neq n. \qquad \text{(Eq. 5)}$$

The eigenvectors only define directions; they are of arbitrary length. Here we choose to normalize the eigenvectors, so that

$$\mathbf{e}^m \cdot \mathbf{e}^m = 1. \qquad \text{(Eq. 6)}$$

The eigenvalues λ_m are real, but they have no particular ordering; we choose an ascending order here $\lambda_1 \leq \lambda_2 \leq \lambda_3$ for specificity.

Let us now examine transformations between geographic space $\mathbf{x}$ and eigen space, which we designate $\mathbf{z}$. A transformation matrix $\mathbf{E}$ can be constructed from a columnar arrangement of the eigenvectors $\mathbf{e}^m$. We choose to arrange the eigenvector columns in the order of their ascending eigenvalues,

$$\mathbf{E} = \begin{pmatrix} e_1^1 & e_1^2 & e_1^3 \\ e_2^1 & e_2^2 & e_2^3 \\ e_3^1 & e_3^2 & e_3^3 \end{pmatrix}. \qquad \text{(Eq. 7)}$$

The matrix $\mathbf{E}$ is orthonormal, and therefore its inverse is equal to its transpose,

$$\mathbf{E}^{-1} = \mathbf{E}^{\mathrm{T}}. \qquad \text{(Eq. 8)}$$

The matrix $\mathbf{E}$ rotates data from the eigenspace $\mathbf{z} = (z_1, z_2, z_3)$ into the original geographic space $\mathbf{x} = (x_1, x_2, x_3)$ through the transformation

$$\mathbf{x}(i) = \mathbf{E}\mathbf{z}(i). \qquad \text{(Eq. 9)}$$

The inverse transformation is given by

$$\mathbf{z}(i) = \mathbf{E}^{\mathrm{T}}\mathbf{x}(i). \qquad \text{(Eq. 10)}$$

The matrix $\mathbf{E}$ also diagonalizes the covariance matrix, so that

$$\mathbf{E}^{\mathrm{T}}\mathrm{C}\mathrm{E} = \Lambda, \qquad \text{(Eq. 11)}$$

where

$$\Lambda = \begin{pmatrix} \lambda_1 & 0 & 0 \\ 0 & \lambda_2 & 0 \\ 0 & 0 & \lambda_3 \end{pmatrix}. \qquad \text{(Eq. 12)}$$

All of these transformations are orthonormal, they are special cases of a more general similarity transformation, for which the trace is invariant, and so

$$\mathrm{tr}(\mathrm{C}) = \mathrm{tr}(\Lambda) = \sum_m \lambda_m. \quad \text{(Eq. 13)}$$

The eigenvectors and values have an important geometric interpretation. The variance of the data about the reference point $\mathbf{r}$ is an ellipsoid, which has the following simple expression in eigenspace

$$\frac{z_1^2}{\lambda_1} + \frac{z_2^2}{\lambda_2} + \frac{z_3^2}{\lambda_3} = 1. \quad \text{(Eq. 14)}$$

Depending on the relative sizes of the eigenvalues, different symmetries of the data distribution are revealed; a summary is given in Table P2. Note that each eigenvalue λ_m is the variance of the data along the direction defined by its corresponding eigenvector $\mathbf{e}^m$. If λ_3 is the largest eigenvalue, then the major axis is defined as the line segment joining the two points $\pm\sqrt{\lambda_3}\mathbf{e}^3$; the two other shorter minor axes are defined similarly. The eccentricity of each ellipsoidal equator is measured by

$$\epsilon_{mn} = \sqrt{1 - \frac{\lambda_m}{\lambda_n}}, \quad \text{for} \quad m < n. \quad \text{(Eq. 15)}$$

The overall anisotropy of the variance can be roughly quantified by the most eccentric ellipsoidal equator ϵ_{13}. Finally, it is important to recognize the fact that the line parallel to $\mathbf{e}^3(\mathbf{r})$ is, in a least-squares sense, the best fitting line to the data that passes through the reference point $\mathbf{r}$, with $\lambda_3(\mathbf{r})$ being a measure of the misfit to this line. Moreover, the plane normal to $\mathbf{e}^1(\mathbf{r})$, and which contains $\mathbf{e}^2(\mathbf{r})$ and $\mathbf{e}^3(\mathbf{r})$, is the least-squares, best fitting plane to the data that contains the reference point $\mathbf{r}$, with $\lambda_2(\mathbf{r}) + \lambda_3(\mathbf{r})$ functioning as a measure of misfit.

It is of interest to translate the eigenvalues into more conventionally interpretable quantities. For a prolate variance ellipsoid, Kirschvink (1980) has defined an approximate maximum angular deviation ($\mathrm{MAD_p}$) from the major axis $\mathbf{e}^3(0)$ by the conic angle determined by a projection of the minor ellipse onto the unit sphere

$$\mathrm{MAD_p} = \tan^{-1}\left[\sqrt{\frac{\lambda_1(0) + \lambda_2(0)}{\lambda_3(0)}}\right], \text{for} \quad \lambda_1 \simeq \lambda_2 \ll \lambda_3. \quad \text{(Eq. 16)}$$

For an oblate variance ellipsoid, we can also define a corresponding maximum angular deviation ($\mathrm{MAD_o}$) from the plane normal to the most minor axis along $\mathbf{e}^1(0)$,

$$\mathrm{MAD_o} = \tan^{-1}\left[\sqrt{\frac{\lambda_1(0)}{\lambda_2(0) + \lambda_3(0)}}\right], \quad \text{for} \quad \lambda_1 \ll \lambda_2 \simeq \lambda_3, \quad \text{(Eq. 17)}$$

which is somewhat different from the definition offered by Kirschvink. With respect to the maximum intensity deviation, if the variance ellipsoid about $\mathbf{r} = \bar{\mathbf{x}}$ is more or less spherical, then the maximum intensity deviation (MID) can be estimated as

Table P2 Eigenvalue classifications

Eigenvalues	Eigenvectors	Variance ellipsoid
$\lambda_1 = \lambda_2 = \lambda_3$	No preferred orientation	Spherical
$\lambda_1 = \lambda_2 < \lambda_3$	$\mathbf{e}^1$ and $\mathbf{e}^2$ have no preferred orientation	Prolate ellipsoid with rotational symmetry about $\mathbf{e}^3$
$\lambda_1 < \lambda_2 = \lambda_3$	$\mathbf{e}^2$ and $\mathbf{e}^3$ have no preferred orientation	Oblate ellipsoid with rotational symmetry about $\mathbf{e}^1$
$\lambda_1 \neq \lambda_2 \neq \lambda_3$	All eigenvectors have definite orientation	Scalene ellipsoid, with no axis of symmetry

Table P3 Principal component analysis of the Hawaiian data

Reference	Eigenvalue (μT^2)	Eigen direction $I(^\circ)$	Eigen direction $D(^\circ)$	Eccentricities ϵ_{12}	Eccentricities ϵ_{23}	Eccentricities ϵ_{13}	MID (μT)	$\mathrm{MAD_p}$ ($^\circ$)
			Past 5 Ma, Full vectors					
	34.4 (μT^2)	10.0	–96.4					
$r = 0$	65.6 (μT^2)	55.7	158.8	0.69				15.0
	1384.2 (μT^2)	32.5	0.1					
			Brunhes only, Full vectors					
	26.2 (μT^2)	12.5	–94.6					
$r = 0$	52.1 (μT^2)	54.2	157.5	0.71				12.8
	1505.4 (μT^2)	32.9	3.7					
	24.1 (μT^2)	11.4	–83.9					
$r = \bar{x}$	47.2 (μT^2)	44.3	174.7	0.70	0.81	0.91	11.8	
	138.4 (μT^2)	43.5	17.1					
			Past 5 Ma, Directions only					
	0.0304	–14.6	87.6					
$r = 0$	0.0601	–58.9	–48.4	0.71				17.6
	0.9088	31.1	–1.5					

Note: Results are shown for data recording a mixture of normal and reverse polarities over the past 5 Ma, as well as for normal Brunhes data only. Covariance is measured relative to the origin $\boldsymbol{r} = (0, 0, 0)$ and, for Brunhes data, relative to the vectorial mean $\bar{\boldsymbol{x}} = (31.3, 15.4, 19.7)\mu$T. The direction-only analysis utilizes unit vectors of the 5 Ma data set.

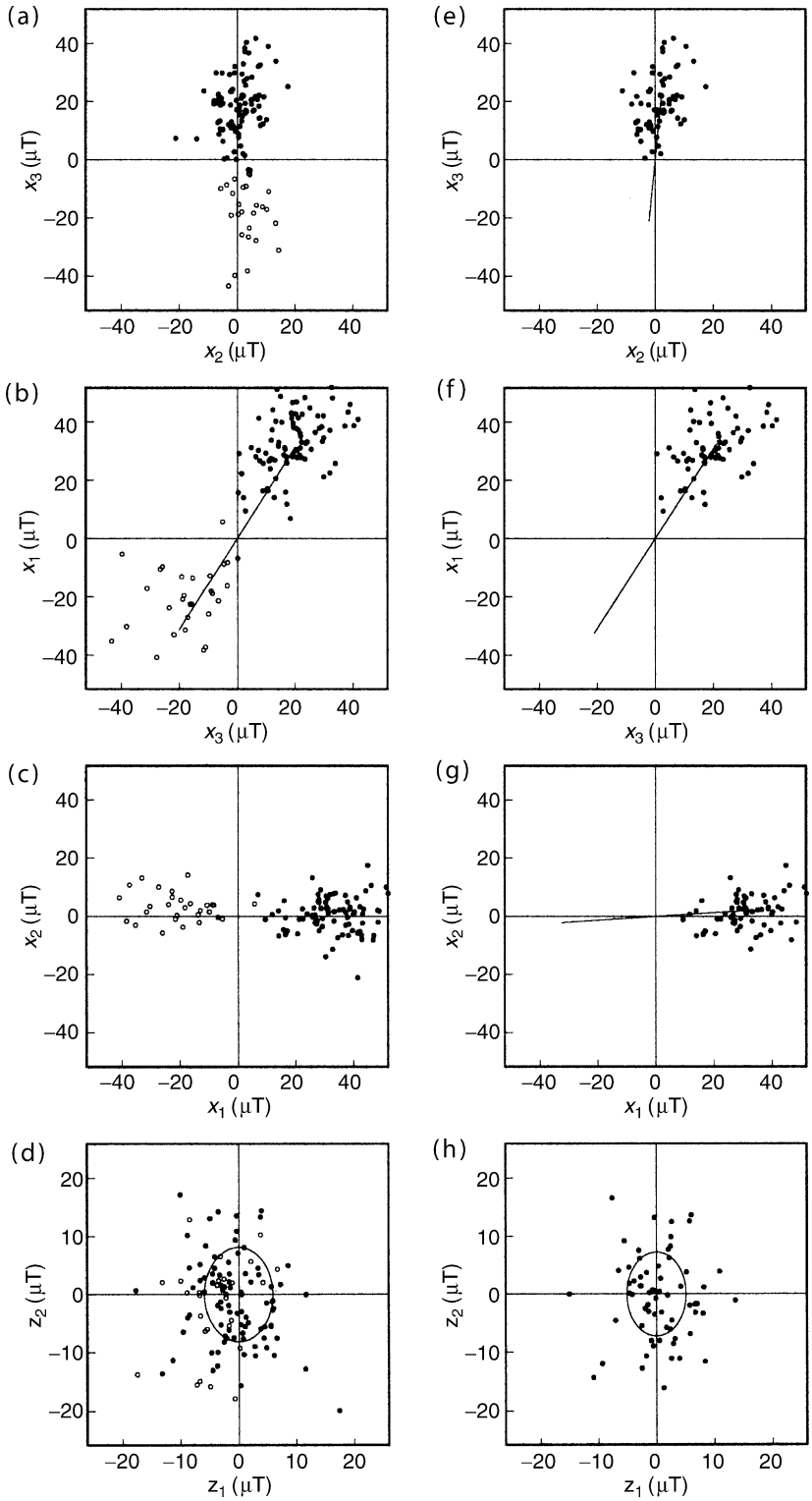

Figure P59 Projection of Hawaiian paleovector data onto the three geographic planes defined by (x_1,x_2,x_3) and onto the eigenplane $z_1 - z_2$ normal to the direction of the major axis defined by $\mathbf{e}^3$. (a-d) show data covering the past 5 Ma. (e-f) show data covering the normal Brunhes. In (a-c) and (e-f) we plot the major axis, and in (d) and (h) we plot the projection of the variance ellipse. Solid circles (disks) represent normal data, open circles represent reversed data.

$$\text{MID} = \sqrt{\frac{\lambda_1(\overline{\mathbf{x}}) + \lambda_2(\overline{\mathbf{x}}) + \lambda_3(\overline{\mathbf{x}})}{3}}, \quad \text{for} \quad \lambda_1 \simeq \lambda_2 \simeq \lambda_3. \tag{Eq. 18}$$

Otherwise, for aspherical dispersion, we need to consider the projection of the variance onto $\mathbf{e}^3(0)$,

$$\text{MID} = \sqrt{\sum_m \lambda_m(\overline{\mathbf{x}})[\mathbf{e}^m(\overline{\mathbf{x}}) \cdot \mathbf{e}^3(0)]^2}. \tag{Eq. 19}$$

Hawaiian bimodal vectors

Let us now illustrate the utility of principal component analysis with paleomagnetic data. For this example, we consider Hawaiian paleomagnetic vector data coming from lava flows emplaced over the past 5 Ma (Love and Constable, 2003), a period of time that encompasses several periods of normal and reverse field polarity. We consider only those flows that, upon sampling and subsequent measurement, have yielded complete triplets of intensity, inclination, and declination ($F(i)$, $I(i)$, $D(i)$), and which, therefore, represent the full ambient magnetic vector at the time of deposition. Calculating the covariance matrix about the origin, using $\mathbf{r} = 0$ in Eq. (3), we perform a principal component analysis to obtain the eigenvalues and corresponding eigenvectors; see Table P3. The major axis along $\mathbf{e}^3$ is orientated almost parallel to the mean direction found by others using other methodologies. This axis is shown in Figure P59a-P59c, where we see that it passes through both the zero point origin and the cloud of points defining the paleosecular variation. As a physical interpretation, it is this axis about which the geomagnetic field varies over time and, even, occasionally reverses its polarity. In Figure P59d we show the projection of the data onto the eigenplane $z_1 - z_2$, where we also plot the variance ellipse defined by the projection of the variance ellipsoid.

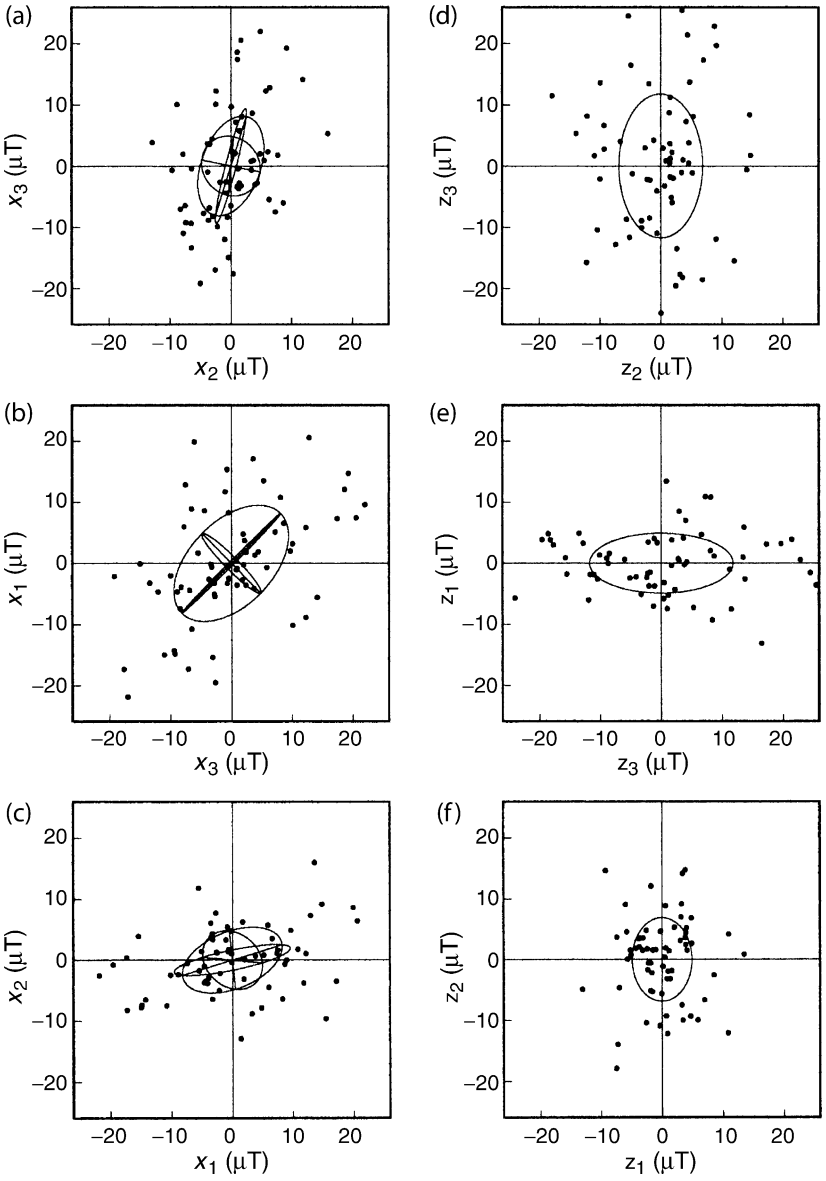

Figure P60 Projection of Brunhes Hawaiian paleovector secular-variation data (with mean vector having been subtracted) onto (a-c) the three geographic planes defined by (x_1, x_2, x_3) and onto (d-f) the three eigenplanes defined by (z_1, z_2, z_3). Also shown are the projections of the three equators of the variance ellipsoid in each coordinate system.

The slightly asymmetric form of the paleosecular variation about the major axis is to be noted.

Hawaiian unimodal vectors

Next, let us consider Brunhes normal data from Hawaii. Results of a principal component analysis of these data for reference point r = 0 are given in Table P3. In Figure P59e-P59g we plot the major axis defined by $\mathbf{e}^3$, and in Figure P59h we show the projection of the data onto the eigenplane $z_1 - z_2$, along with the corresponding variance ellipse. The results here are not dramatically different from the previous result, where we used data of mixed polarities, although some slight differences in the orientation of the major axis and variance size are noted. In order to better inspect the nature of the paleosecular variation at Hawaii during the Brunhes, we perform a principal component analysis of the covariance about the mean vector $\mathbf{r} = \overline{\mathbf{x}}$. In Table P3 we see that much of the secular variation is roughly parallel with the mean vector; the angular difference between the orientation of the two vectors is only 14.9°. The geometric form of the variance of the secular variation is shown in Figure P60, where we plot both the data and the variance ellipse in geographic and eigencoordinates. The utility of measuring the variance about the vectorial mean $\mathbf{r} = \overline{\mathbf{x}}$ and in the eigenspace $\mathbf{z}$ should now be obvious.

Directional analysis

Usually, paleomagnetists do not have complete vectorial data. Instead, directional data, consisting of inclination and declination values ($I(i)$, $D(i)$), are most commonly available. Therefore, let us consider a principal component analysis for directional-only data. The equivalent Cartesian expression of the data is

$$\begin{aligned}\hat{x}_1(i) &= \cos I(i) \cos D(i),\\ \hat{x}_2(i) &= \cos I(i) \sin D(i),\\ \hat{x}_3(i) &= \sin I(i).\end{aligned} \qquad \text{(Eq. 20)}$$

With N such directional data we can calculate their covariance about the defined origin $\mathbf{r} = (0, 0, 0)$

$$\hat{\mathbf{C}} = \frac{1}{N}\begin{pmatrix} \sum \hat{x}_1(i)^2 & \sum \hat{x}_1(i)\hat{x}_2(i) & \sum \hat{x}_1(i)\hat{x}_3(i) \\ \sum \hat{x}_2(i)\hat{x}_1(i) & \sum \hat{x}_2(i)^2 & \sum \hat{x}_2(i)\hat{x}_3(i) \\ \sum \hat{x}_3(i)\hat{x}_1(i) & \sum \hat{x}_3(i)\hat{x}_2(i) & \sum \hat{x}_3(i)^2 \end{pmatrix}. \qquad \text{(Eq. 21)}$$

As before, eigenvalues λ_m and eigenvectors $\mathbf{e}^m$ can be obtained for this matrix. Because all the data are unit vectors, the total variance measured relative to the origin is one and the trace of $\hat{\mathbf{C}}$ is unity:

$$\mathrm{tr}(\hat{\mathbf{C}}) = 1, \qquad \text{(Eq. 22)}$$

and so the sum of the three eigenvalues is determined,

$$\lambda_1 + \lambda_2 + \lambda_3 = 1. \qquad \text{(Eq. 23)}$$

This means that the eigenvalues have only two degrees of freedom. For a prolate variance ellipsoid, the approximate maximum angular deviation from the major axis along $\mathbf{e}^3$ is

$$\mathrm{MAD}_\mathrm{p} = \tan^{-1}\left[\sqrt{\frac{1-\lambda_3}{\lambda_3}}\right], \qquad \text{(Eq. 24)}$$

and for an oblate variance ellipsoid, the corresponding angular deviation from the plane normal to $\mathbf{e}^1$ is

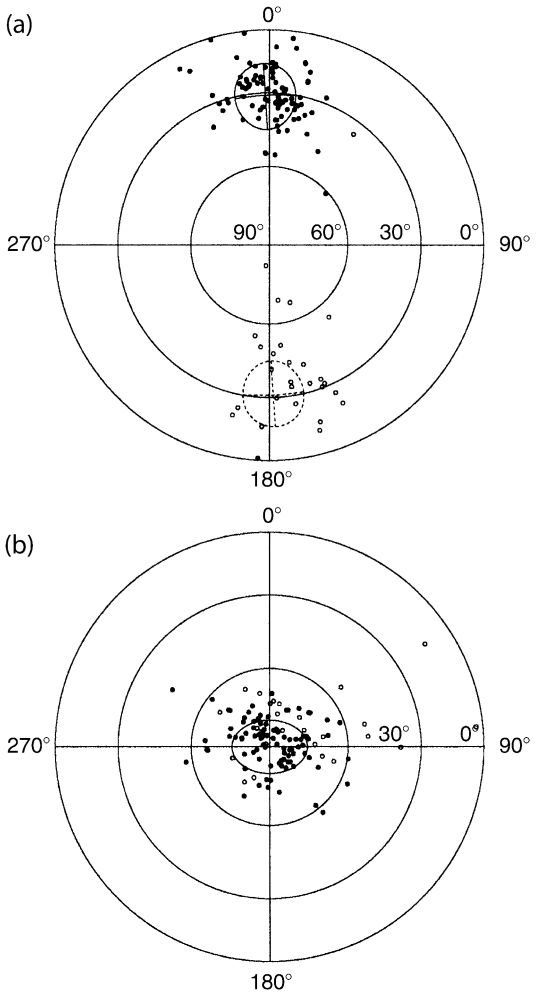

Figure P61 Equal-area projection of Hawaiian directional data, defined in (a) geographic coordinates and (b) eigen coordinates. Also shown are the projections of the variance minor ellipse, defined by λ_1 and λ_2. As is conventional, the azimuthal coordinate is declination (clockwise positive, 0°–360°), and the radial coordinate is inclination (from 90° in the center to 0° on the circular edge).

$$\mathrm{MAD}_\mathrm{o} = \tan^{-1}\left[\sqrt{\frac{\lambda_1}{1-\lambda_1}}\right]. \qquad \text{(Eq. 25)}$$

Hawaiian bimodal directions

As a final example, we return to the mixed polarity Hawaiian data covering the past 5 Ma, but this time we only consider the paleodirections $(I(i), D(i))$. Results of a principal component analysis of the corresponding unit vectors for reference point $r = 0$ are given in Table P3. In Figure P61a we plot the data, and the minor ellipse defined by λ_1 and λ_2, in an equal-area projection of geographic coordinates. After rotation into eigenspace (Figure P61b), we see, quite clearly, the asymmetric variance of paleodirections, thus, demonstrating the utility of inspecting directional data in the eigenspace $\mathbf{z}$.

Jeffrey J. Love

Bibliography

Hotelling, H., 1933. Analysis of a complex of statistical variables into principal components. *Journal of Educational Psychology*, **24**: 417–441, 498–520.

Jolliffe, I.T., 2002. *Principal Component Analysis*, 2nd edn. New York: Springer-Verlag.

Karhunen, K., 1947. Über lineare Methoden in der Wahrscheinlichkeitsrechnung. *Annales Academiae Scientiarum Fennocaeseries A1*, **37**: 3–79.

Kirschvink, J.L., 1980. The least-squares line and plane and the analysis of palaeomagnetic data. *Geophysical Journal International*, **62**: 699–718.

Loéve, M., 1977. *Probability Theory*, 4th edn. New York: Springer-Verlag.

Love, J.J. and Constable, C.G., 2003. Gaussian statistics for palaeomagnetic vectors. *Geophysical Journal International*, **152**: 515–565.

Mardia, K.V., 1972. *Statistics of Directional Data.* New York: Academic Press.

Pearson, K., 1901. On lines and planes of closest fit to systems of point in space. *Philosophical Magazine*, *series 6,* **2**: 559–572.

Schomaker, V., Wasser, J., Marsh, R.E. and Bergman, G., 1959. To fit a plane or a line to a set of points by least squares. *Acta crystallographica*, **12**: 600–604.

Strang, G., 1980. *Linear Algebra and Its Applications*, New York: Academic Press.

Cross-references

Bingham Statistics
Fisher Statistics
Magnetic Remanence, Anisotropy
Paleomagnetic Secular Variation
Statistical Methods for Paleovector Analysis

PROJECT MAGNET

Project Magnet is a comprehensive vector aeromagnetic surveying enterprise that spanned much of the last five decades. Under the direction of the United States Navy and management by the Naval Oceanographic Office, test flights began in 1951 and full operational capabilities were established in 1953. The project ran through 1994, ultimately contributing many thousands of track miles (see Figure P62) of geomagnetic data (Coleman, 1992). The data are available on CD-ROM through the National Geophysical Data Center (Hittelman *et al*., 1996).

The primary purpose of Project Magnet was to supply data in support of the World Magnetic Modeling (WMM) and charting program, which in turn supported civilian and military navigation requirements. The WMM has been incorporated into many global positioning system (GPS) receivers manufactured in the United States and has been used to control drift rates in inertial navigation systems. As a geophysical tool, the WMM has been useful as a reference measurement for Earth's core–mantle boundary field and as an aid in geophysical prospecting and resource evaluation.

Over the years, Project Magnet surveys have been performed using five different aircrafts, with each successive one improving in range, speed or altitude, navigational capabilities, and geophysical instrumentation. From 1953 to 1970 survey aircraft flew at 4615 m and most surveys were confined to remote ocean areas. Navigation methods in use at the time were periodic celestial fixes, LORAN, and dead reckoning. As a result, navigational accuracy was rather poor and was limited to about 5 nautical miles. Altitudes were determined using a baroclinic altimeter, with an uncertainty of ± 30 m. Observations of declination, inclination, and intensity (to an accuracy of ± 15 nT) were made using a self-orienting fluxgate magnetometer, while a towed, optically pumped metastable helium magnetometer measured field intensity to ± 4 nT. Until 1970, data acquisition systems consisted primarily of strip chart recorders and navigation logs. The majority of this data has been manually digitized.

The introduction of a new aircraft in 1970 permitted high level (over 4615 m) vector aeromagnetic surveying, usually conducted at altitudes between 6200 and 7700 m. During this era, the use of inertial navigation systems improved navigational accuracy to about 1 nautical mile, and in 1987, after the appearance of GPS, accuracies were further increased to several tens of meters, but only when a reliable signal was available. A baroclinic altimeter similar to the previous one was again the only source of altitude data. Improved magnetic measurements were facilitated by a fluxgate magnetometer, providing three vector components X, Y, and Z in the local reference frame to accuracies of ± 40 nT. An optically pumped metastable helium magnetometer mounted on a stinger extending from the rear of the aircraft measured intensity to ± 1 nT.

Major technological improvements arrived with the 1990s and by 1992 the Project Magnet aircraft had been fitted with an ASG-81 scalar magnetometer, a NAROD ring-core fluxgate vector magnetometer, and a ring-laser gyro (RLG) inertial system. The latter two instruments were mounted on a rigid beam in a magnetically clean area at the rear of the aircraft. The RLG was used primarily for attitude determination, while GPS, a radar system and a precision barometer were employed for altitude measurements, which were determined to a precision of less than 2 m. The GPS system was the primary navigational tool, with a circular error probability of 15 m. However, the accuracy of the magnetic measurements remained the same. Technological advancements also led to the incorporation of a number of other surveying capabilities, including gravity, ocean acoustics, and ocean temperature.

Survey data were calibrated by several low level "airswings" prior to and during the high level surveying. The airswings included straight and level passes as well as roll, pitch and yaw maneuvers in each cardinal direction at 1000 feet over a ground based observatory. The calibration data were used to model aircraft intrinsic magnetic fields that perturb the magnetometer data. The contaminating fields are due to: the permanently magnetized part of the aircraft; magnetization induced by the core field; and eddy currents driven by changes in the crustal and core fields as the aircraft passed through them. A compensation model, based on developments by Leliak (1961), involves a two-step iterative least squares solution for 21 coefficients, which characterize the contaminating fields, and three bias angles, which account for differences in the orientations of the vector magnetometer and the inertial navigation system. Measurements taken over all airswing maneuvers are then included in a least squares minimization of the difference between the magnitudes of the decontaminated aeromagnetic observations and the transformed ground based observations. This transformation involves upward continuation to aircraft altitude and rotation into the aircraft reference frame using roll, pitch and heading data.

The compensation model is imprecise in that it is based on the assumption that the coefficients are constant with respect to latitude and frequency of the airswing maneuvers. There have been attempts to account for these variations and the Project Magnet database includes compensation coefficients from repeated calibration flights at observatories over the globe. More importantly, Project Magnet orientation accuracy is insufficient to prevent contamination of the magnetic field vector components due to misalignment of the aircraft coordinate system (Parker and O'Brien, 1997). Because field intensity is immune from orientation errors, Parker and O'Brien (1997) show that simple spectral analysis of intensity and the three vector magnetic components as functions of along track distance may be used as a diagnostic for this contamination.

Although one of the primary goals of Project Magnet was to characterize the magnetic field generated in Earth's core, the majority of published studies exploiting Project Magnet data have been focused on the crustal part of the field, including numerous regional magnetic